Arctic Cyclone Activity and the Beaufort High

JESSICA S. KENIGSON^a AND M.-L. TIMMERMANS^a

^a Department of Earth and Planetary Sciences, Yale University, New Haven, Connecticut

(Manuscript received 2 October 2020, in final form 9 February 2021)

ABSTRACT: The Beaufort high (BH) and its accompanying anticyclonic winds drive the Arctic Ocean's Beaufort Gyre, the major freshwater reservoir of the Arctic Ocean. The Beaufort Gyre circulation and its capacity to accumulate or release freshwater rely on the BH intensity. The migration of Nordic seas cyclones into the Arctic has been hypothesized to moderate the strength of the BH. We explore this hypothesis by analyzing reanalysis sea level pressure fields to characterize the BH and identify and track cyclones north of 60°N during 1948–2019. A cluster analysis of Nordic seas cyclone trajectories reveals a western pathway (through the Arctic interior) associated with a relatively weak BH and an eastern pathway (along the Arctic periphery) associated with a relatively strong BH. Furthermore, we construct cyclone activity indices (CAIs) in the Arctic and Nordic seas that take into account multiple cyclone parameters (number, strength, and duration). There are significant correlations between the BH and the CAIs in the Arctic and Nordic seas during 1948–2019, with anomalously strong cyclone activity related to an anomalously weak BH, and vice versa. We show how the Arctic and Nordic seas CAIs experienced a regime shift toward increased cyclone activity between the first four decades analyzed (1948–88) and the most recent three decades (1989–2019). Over the same two time periods, the BH exhibits a weakening. Increased cyclone activity and an accompanying weakening of the BH may be consistent with expectations in a warming Arctic and have implications for Beaufort Gyre dynamics and freshwater.

KEYWORDS: Atmosphere; Arctic; Atmosphere-ocean interaction; Extratropical cyclones

1. Introduction

The Arctic sea level pressure (SLP) field may be approximately characterized by a large-scale high pressure system in the west [the anticyclonic Beaufort high (BH)] and a low pressure system in the east extending from the Icelandic low (Serreze and Barrett 2011). The anticyclonic winds associated with the BH drive the convergence of relatively fresh waters in the oceanic Beaufort Gyre, the Arctic Ocean's major freshwater reservoir (e.g., Proshutinsky et al. 2009; Haine et al. 2015). The strength and variability of the BH therefore influence sea ice cover and regulate freshwater fluxes between the Arctic and North Atlantic. The Icelandic low is a locus of intense cyclone activity in the vicinity of the Nordic seas, reflecting the passage of storms along the principal North Atlantic storm track (Serreze et al. 1997; Sorteberg and Walsh 2008). Cyclones flux vorticity and moisture to the Arctic from lower latitudes, and Icelandic low cyclones have an outsized role in the transport (Sorteberg and Walsh 2008; Villamil-Otero et al. 2018). Cyclone activity is believed to play an important role in the variability of the BH, although the relationship is not well understood. In this study, we characterize Arctic cyclone activity for the 1948–2018 period and explore its statistical relationship with the BH.

Kenigson's current affiliation: Department of Applied Mathematics, University of Colorado Boulder, Boulder, Colorado.

Corresponding author: J. S. Kenigson, jessica.kenigson@colorado.edu

Some general hypotheses for the relationship between the confluence of cyclone activity that characterizes the Icelandic low and the BH have been suggested. For example, an idealized decadal climate oscillation scenario was put forward by Proshutinsky et al. (2015): When the BH wind forcing is anomalously strong (i.e., favorable for freshwater convergence), the freshwater flux from the Arctic to the Nordic seas declines, the Nordic seas are preconditioned for deep convective mixing, and the ocean-to-atmosphere heat flux increases, favoring cyclone intensification and/or cyclogenesis. These cyclones, in turn, are hypothesized to propagate into the Arctic and weaken the BH, allowing for the release of freshwater from the Beaufort Gyre, and the cycle repeats. Examination of whether such a scenario plays out first requires understanding the field of Nordic seas cyclone activity in context with the interannual to decadal variability of the atmospheric BH, and that is the focus of this paper.

Arctic cyclone activity has been examined in a number of studies (e.g., Bell and Bosart 1989; Serreze and Barry 1988; Serreze et al. 1993; Serreze 1995; Gulev et al. 2001; McCabe et al. 2001; Zhang et al. 2004; Sorteberg and Walsh 2008; Sepp and Jaagus 2011). Zhang et al. (2004) quantified Arctic and midlatitude cyclone activity during 1948–2002, considering both the number of cyclone centers and the mean cyclone intensity, which together contribute to a cyclone activity index (CAI; see section 2). Their analysis indicates significant interannual to multidecadal variability of the CAI during the study period, with a trend toward increasing cyclone activity during ~1970–90. Sepp and Jaagus (2011) found a significant positive trend in the count of cyclones entering the Arctic from the subarctic; about 44 more per year were incident in 2002 than 1948, with a mean of about 203 per year during that period. At

the same time, linear trends suggested that deep cyclones (central pressure less than 1000 hPa) were becoming more frequent, and shallow cyclones less frequent. Sorteberg and Walsh (2008) detected significant positive linear trends (about 3% per decade) in cyclone activity, as defined by the positive vorticity accumulated in the Arctic, in all seasons but winter during 1948-2002. These findings are consistent with a northward shift of zones of maximum baroclinicity and storm tracks in a warming climate, as have been found in certain climate model simulations (Yin 2005); we note, however, that more recent climate model ensembles suggest varying and somewhat inconsistent projections for the Northern Hemisphere storm track (Chang and Yau 2016; Harvey et al. 2020). Nordic seas cyclones accounted for ~30% of the positive vorticity accumulated in the Arctic by incident cyclones (i.e., across 70°N) during the 1948-2002 period (Sorteberg and Walsh 2008). The number of Nordic seas cyclones (within 20°W-20°E) entering the Arctic was increasing during that period, although the trend did not reach statistical significance (Sepp and Jaagus 2011).

A few studies have considered the relationship between the BH and cyclone activity. For example, Hori et al. (2015) considered summer-only and attributed the interannual variability of the summer BH to the influx of cyclonic storms. However, the BH is weakly defined or absent in summer relative to winter (Serreze and Barrett 2011). A case study linked the weakening of the BH in the winter of 2017 to the influx of cyclones along the North Atlantic storm track (Moore et al. 2018), suggesting a linkage that may hold in general. Here we investigate whether such connections may be generalized by exploring the relationship between annual-mean cyclone activity (with a focus on the Nordic seas) and the BH over an approximately 70-yr period (1948–2019).

The paper is outlined as follows. In the next section, we outline the methodology for characterizing SLP centers of action, identifying and tracking cyclones in the Arctic and subarctic north of 60°N, and constructing CAIs. In section 3, we show how the BH strength is inversely correlated with the strength and extent of the Icelandic low in the Arctic. Specifically, we use a cluster analysis on Icelandic low cyclone trajectories to investigate how storm activity relates to the Arctic SLP field. In section 4, we quantify the covariability of the BH and Nordic seas cyclone activity as characterized by CAIs. Furthermore, we show that cyclone activity and the Beaufort high have undergone a coherent multidecadal regime shift. Our results have important implications for the future and fate of Arctic freshwater, as discussed in section 5.

2. Characterizing the Beaufort high and cyclone activity

The BH is characterized using the NCEP–NCAR Reanalysis I SLP field ($2.5^{\circ} \times 2.5^{\circ}$ horizontal resolution; Kalnay et al. 1996) as a spatial mean SLP over the region 135°W–180°, 72.5°–80°N based on the definition of Serreze and Barrett (2011) (Fig. 1a, dash-outlined box).

Cyclones are identified and tracked during 1948–2019 through the application of an algorithm (described next) to the 6-hourly NCEP–NCAR Reanalysis I SLP fields; this reanalysis product has been used in numerous studies to identify and

track cyclones in the Arctic region (e.g., Gulev et al. 2001; Zhang et al. 2004; Sorteberg and Walsh 2008; Rudeva and Gulev 2011; Villamil-Otero et al. 2018). Although the NCEP-NCAR reanalysis data have been used extensively for this purpose, notably, cyclone statistics differ among reanalysis products (Simmonds et al. 2008; Chang and Yau 2016). The various other reanalyses, however, do not cover the same period of record as the NCEP-NCAR data.

Cyclone identification and tracking

There are several cyclone identification/tracking algorithms in the literature (e.g., Serreze et al. 1997; Sorteberg et al. 2005; Rudeva and Gulev 2011), but we have chosen the following general criteria for consistency with Zhang et al. (2004) and Villamil-Otero et al. (2018). We have made minor modifications to these criteria (e.g., by explicitly requiring a positive relative vorticity at cyclone centers).

- The SLP at a cyclone center must be a local spatial minimum.
- 2) The minimum SLP gradient between the cyclone center and the eight surrounding grid points must be at least 0.15 hPa per 100 km. The SLP field at the surrounding grid points is smoothed using a local nine-point smoother (NCAR 2019).
- 3) The mean of the zonal and meridional SLP gradients between the four points in the cardinal directions surrounding the cyclone center and their outside adjacent points in the same cardinal directions must be negative inward. This criterion is designed to eliminate open low pressure systems.
- 4) Cyclone centers located within 1200 km of each other at the same 6-hourly time step are considered redundant. Redundant cyclone centers are iteratively removed in descending order of SLP (i.e., with a preference for retaining the strongest storm systems).
- 5) Cyclone centers must have a negative SLP anomaly (defined as the difference between the SLP at the cyclone center and the long-term mean monthly climatology at the cyclone center grid point) and positive relative vorticity at 850 hPa. Relative vorticity is estimated from the 6-hourly, 850-hPa wind fields.

Cyclone tracking is performed by assigning unique IDs to cyclone centers at cyclogenesis and propagating them forward in time. Specifically, if a cyclone center at a 6-hourly time step is within 600 km of a cyclone center at the previous 6-hourly time step, it is considered to be part of the same cyclone trajectory; otherwise, a new trajectory is generated.

The trajectories of Nordic seas cyclones that enter the Arctic are grouped using a cluster analysis algorithm for streamlines (Garyfallidis et al. 2012). Briefly, each cyclone trajectory is assigned to a cluster if a distance metric between that trajectory and an existing cluster centroid is less than a specified threshold; otherwise, the method instantiates a new cluster. Here the distance metric represents the mean distance between cyclone centers at successive 6-hourly time steps during the initial six days after the cyclones enter the Arctic Ocean. The persistence criterion was empirically chosen to remove relatively short cyclone tracks that do not form well-defined, separated clusters over the cyclone lifetime. The distance threshold was also

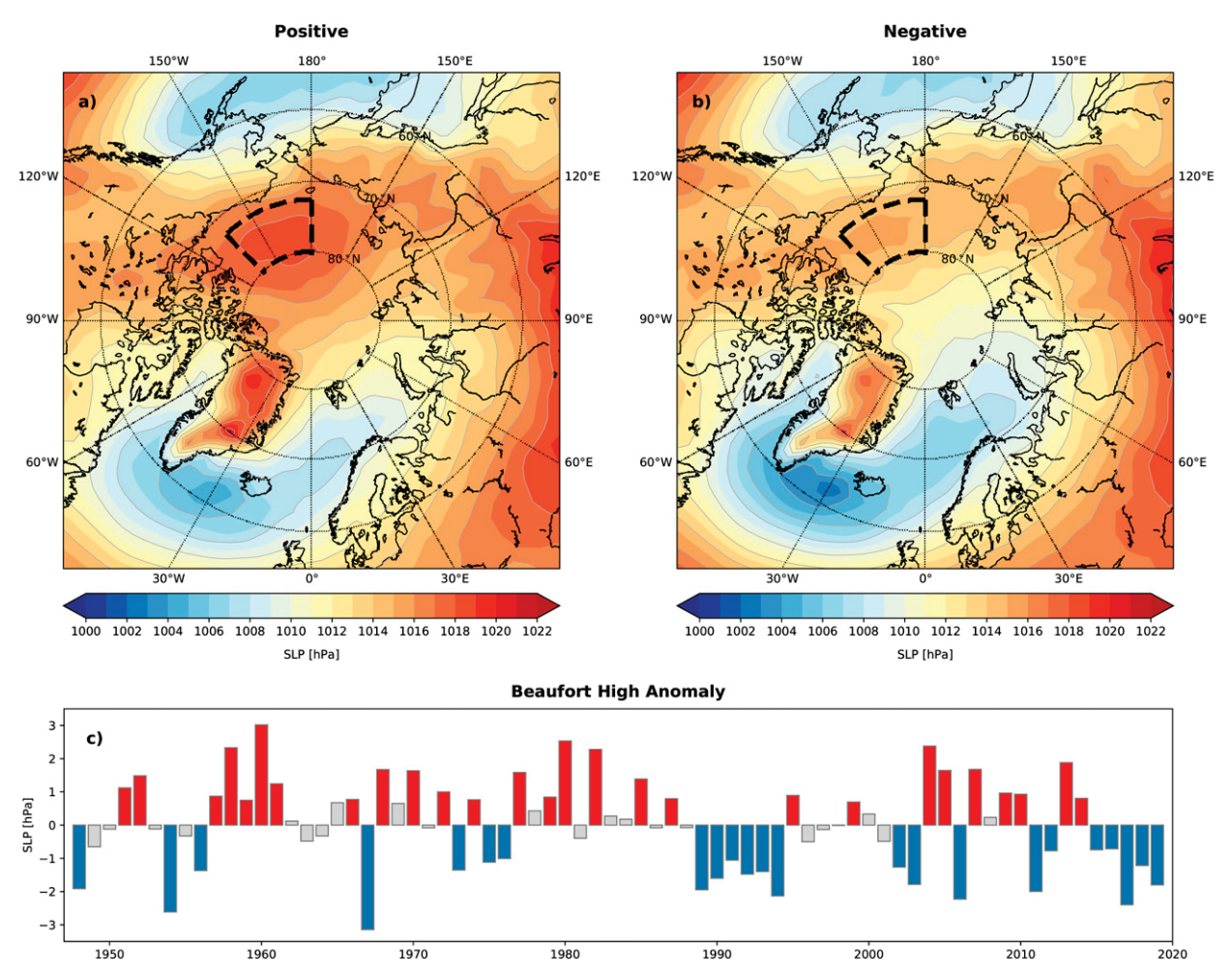


FIG. 1. (a) Composite SLP over years in which the BH was greater than 0.5 standard deviations of its mean during 1948–2019 [red bars in (c)]. The dash-outlined box indicates the center of action of the BH. (b) As in (a), but for years in which the BH was less than -0.5 standard deviations of its mean [blue bars in (c)]. (c) BH SLP anomaly relative to the 1948–2019 mean.

empirically chosen to be 1400 km, but a sensitivity analysis suggests that the centroids are relatively robust to perturbations of this value. Furthermore, our clusters are broadly consistent with those of prior studies that used different identification and clustering algorithms (Sorteberg and Walsh 2008).

Last, we construct SLP-based CAIs (CAI_{SLP}) for the Arctic (defined as the region north of 70°N) and the Nordic seas (60°–77.5°N, 27.5°W–30°E), which reflect the number, strength, and duration of cyclones (Zhang et al. 2004). Specifically, a monthly CAI is constructed by summing the cyclone center SLP anomaly (i.e., the SLP minus the long-term mean monthly climatology at the cyclone center grid point) over all cyclone centers in the 6-hourly data during each month. The negative of the SLP anomaly is defined as the cyclone intensity, and the sign of the CAI is reversed such that a positive CAI anomaly represents an enhancement of cyclone activity. For a given region and time period, the cyclone count is the number of cyclone centers identified in the 6-hourly SLP fields. Therefore, cyclone count depends upon both the number and duration of

cyclones. Since the CAI directly depends upon the ambient SLP, complicating its comparison with the BH, we also construct a vorticity-based CAI (CAI $_{\zeta}$) as the sum of the 850-hPa relative vorticity at all identified cyclone centers in a given period and area; CAI $_{\zeta}$ depends upon the Laplacian of SLP rather than the SLP itself (see Sorteberg and Walsh 2008).

Since the cyclone identification and tracking algorithm is sensitive to choices of parameters and thresholds, a sensitivity analysis to the smoothing parameters in the SLP gradient calculation is performed. Specifically, the analysis is rerun after performing "light" rather than "heavy" smoothing; see details of the nine-point smoothing algorithm in NCAR (2019). Using light smoothing tends to result in shorter cyclone tracks; we analyze the cyclone tracks that result from the heavy smoothing, which are similar to those identified in prior studies (Sorteberg and Walsh 2008). The number of cyclone centers and trajectories is somewhat sensitive to the choice of smoothing parameters, but the normalized CAI is quite insensitive. Furthermore, visual inspection reveals a close

correspondence between our index and the CAI of Zhang et al. (2004) over 60°–90°N, 60°–70°N, and 70°–90°N during the overlapping period of 1948–2002.

3. Cyclone trajectories

The strength of the BH is related to the strength and spatial extent of the Icelandic low, as suggested by a composite analysis of the annual mean SLP field (Fig. 1). The BH is anomalously strong (red bars in Fig. 1c) when the Icelandic low is confined to south of $\sim 70^{\circ}$ N, and weak (blue bars in Fig. 1c) when the Icelandic low intrudes northward into the Arctic interior. Our characterization of cyclone trajectories will illustrate how these spatial patterns of SLP relate to cyclone propagation.

Typical cyclone activity during 1948–2019 can be summarized as follows. About 450 unique cyclones are found in the Arctic (north of 70°N) in an average year (excluding short-lived cyclones with lifetimes less than 12 h). Approximately 28% of those originate south of 70°N, while the remainder result from local cyclogenesis. The mean Arctic cyclone lifetime is about 2 days, and the 10th and 90th percentiles are 12 h and 4 days, respectively. The Nordic seas region accounts for an outsized share of the vorticity of incident cyclones accumulated in the Arctic (Fig. 2a). A mean of about 30 cyclones per year enter the Arctic from the Nordic seas, with a lifetime of around 3 days (from the first point of detection north of 60°N to cyclolysis); the 10th and 90th percentiles of lifetime are 1 and 5.5 days, respectively.

Our cluster analysis considers 62 Nordic seas cyclones with lifetimes of at least six days in the Arctic during 1948–2019. Of these, the majority (94%) belonged to an "east" or a "west" cluster (black trajectories and white trajectory centroids in Fig. 2a), with the remainder belonging to a small number of additional clusters that will be omitted from further analysis [see also the similar division of cyclone tracks in Sorteberg and Walsh (2008) during 1948-2002]. Cyclones having an eastern trajectory (i.e., propagating eastward along the Arctic periphery; 66%) were more prevalent than those characterized by a western trajectory (penetrating into the Arctic interior; 34%). The number of western cyclone trajectories did not have a strong seasonal dependence, while the number of eastern cyclone trajectories was nearly 3 times as great in fall as in spring (see Fig. 2b). This may relate to seasonal shifts in the configuration of isobars that set cyclone steering, although sample sizes are too small to draw broad conclusions.

Composite SLP patterns corresponding to the cyclone tracks in each cluster (Figs. 2c,d) demonstrate that when cyclones penetrate the Arctic interior, the Icelandic low extends over the pole and the BH is relatively weak (Fig. 2c). On the other hand, when cyclones track eastward over the Barents Sea, the Icelandic low has a more zonal orientation and the BH is relatively strong (Fig. 2d). Upper-level (500 hPa) geopotential height contours are indicative of how cyclones are steered by the mean winds. In general, we see that these contours are more zonal for cyclones that comprise the east cluster, and more meridional for the west cluster (Figs. 2c,d); that is, the pattern of geopotential height contours favors cyclone

propagation either along eastern or western pathways. We note, however, that the cluster centroids deviate from parallel with 500-hPa height contours, and this is both because there can be significant short-term (subweekly) variability in these planetary-scale signatures and because there is considerable spread in the individual cyclone trajectories that comprise a cluster. Therefore, the spatial patterns of SLP and geopotential height in Fig. 1 reflect different distributions of cyclone activity; this is further illustrated from a statistical perspective in the next section.

4. Relationship between the Beaufort high and cyclone activity

The correlation coefficient between the BH and the Arctic CAIs during 1948–2019 is r=-0.71 for Arctic CAI_{SLP} and r=-0.44 for Arctic CAI $_\zeta$, which are statistically significant (at the p<0.05 level; Fig. 3). Note that the Arctic Oscillation (AO) index (Thompson and Wallace 1998) is a reasonable proxy for Arctic cyclone activity [e.g., over 1950–2018, the Arctic CAI-SLP is statistically significantly correlated with the AO index taken from NOAA's monthly mean values (NOAA 2020) with correlation coefficient of r=0.85]; see also Zhang et al. (2003).

The Icelandic low represents the dominant locus of cyclone activity north of 60°N (Fig. 4a), and this activity is intensified (diminished) during years in which the BH is weak (strong) (Fig. 4b). During 1948–2019, the BH and Nordic seas CAIs are (significantly) correlated, with r = -0.41 for the Nordic seas CAI_{SLP} and r = -0.32 for the Nordic seas CAI_{ζ}. The correlation is weaker than might be expected given the distinct correspondence between cyclones tracking from the Nordic seas and the strength of the BH; the Nordic seas CAI characterizes cyclone activity in a fixed location, regardless of cyclone lifetime or cyclolysis region, while Nordic seas cyclones must propagate into the Arctic in order to influence the BH. Similar correlations hold if winter (January-March) and summer (July-September) are considered separately, with the exception being that there is no statistically significant relationship between the BH and Nordic seas cyclone activity in summer. This suggests that local cyclogenesis and/or the migration of cyclones from other regions play a larger role in summer BH variability than Nordic seas cyclones. For example, the relatively low SLP that predominates in the central Arctic in summer (see also Zhang et al. 2004; Serreze and Barrett 2008) reflects local cyclogenesis and an influx of storms (primarily from the Eurasian continent broadly), due to the enhancement of baroclinicity that results from the differential heating of the ocean and seasonally snow-free land.

The CAI indices suggest that the Arctic as a whole and the Nordic seas in particular experienced intensified cyclone activity between 1948–88 and 1989–2019, attributable to an increase in both the cyclone center count and intensity (see black solid and dashed lines in Figs. 3a,c). Specifically, the Nordic seas CAI_{ζ} increased by over one standard deviation between these periods (and similar for the Arctic CAI_{ζ} ; see Figs. 3b,d). Between the periods 1948–88 and 1989–2019, the mean number of Nordic seas cyclones entering the Arctic each year, and

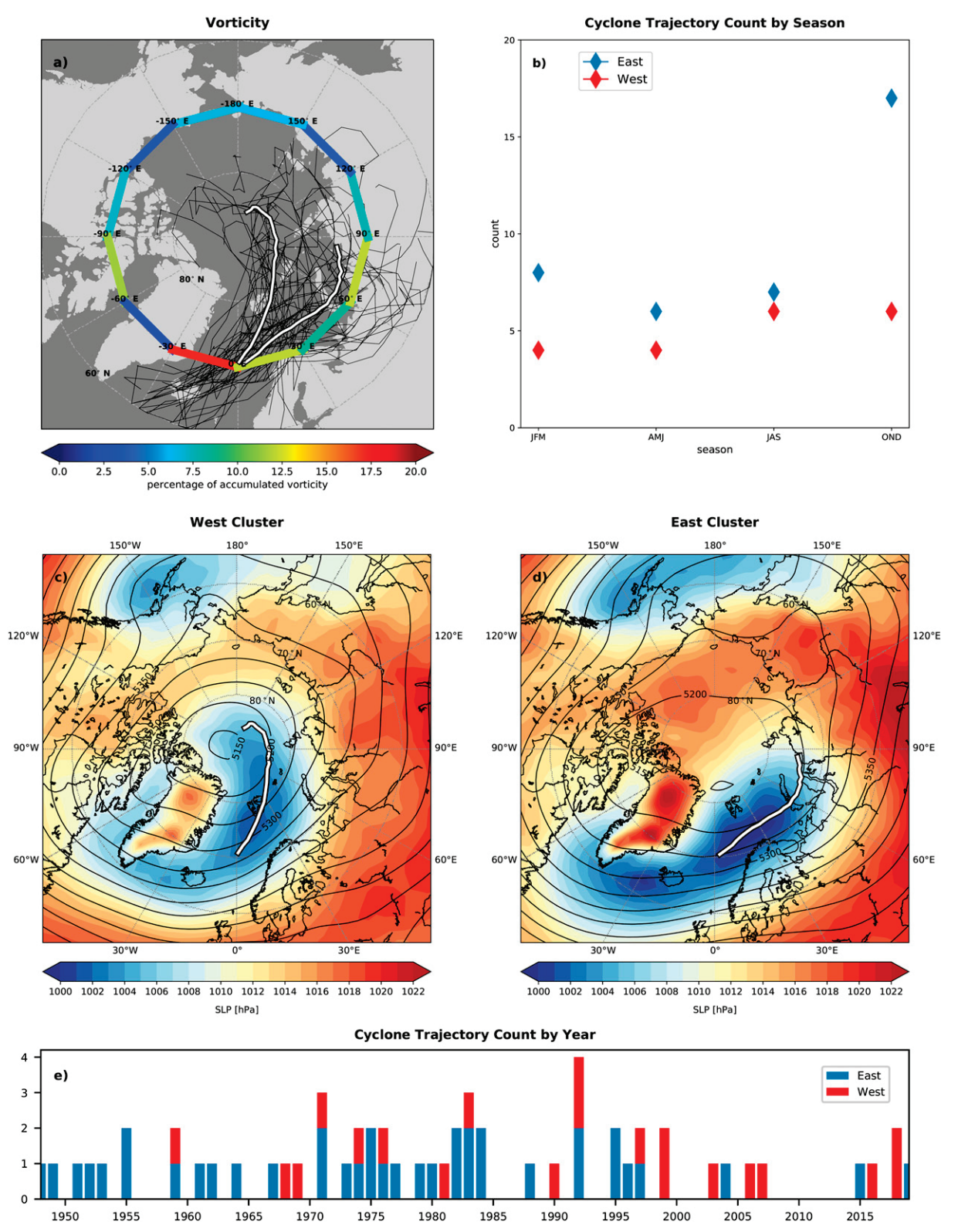


FIG. 2. (a) Percentage of mean (1948–2019) accumulated positive vorticity (850 hPa) for cyclones crossing into the Arctic (i.e., 70°N) in each 30° longitude sector (color shades). Very short-lived cyclones (i.e., with a lifetime less than 12 h) are removed. Also shown are trajectories of cyclones entering the Arctic from the Nordic seas sectors (27.5°W–30°E) belonging to two major clusters (solid black lines, smoothed) and the cluster centroids (solid white lines). (b) Cyclones per cluster by season. Composite SLP over 6-hourly time steps of all cyclones in the (c) west and (d) east clusters. Black lines represent the composite 500-hPa isobars in 50-hPa increments. (e) Numbers of cyclone trajectories in the east and west clusters by year.

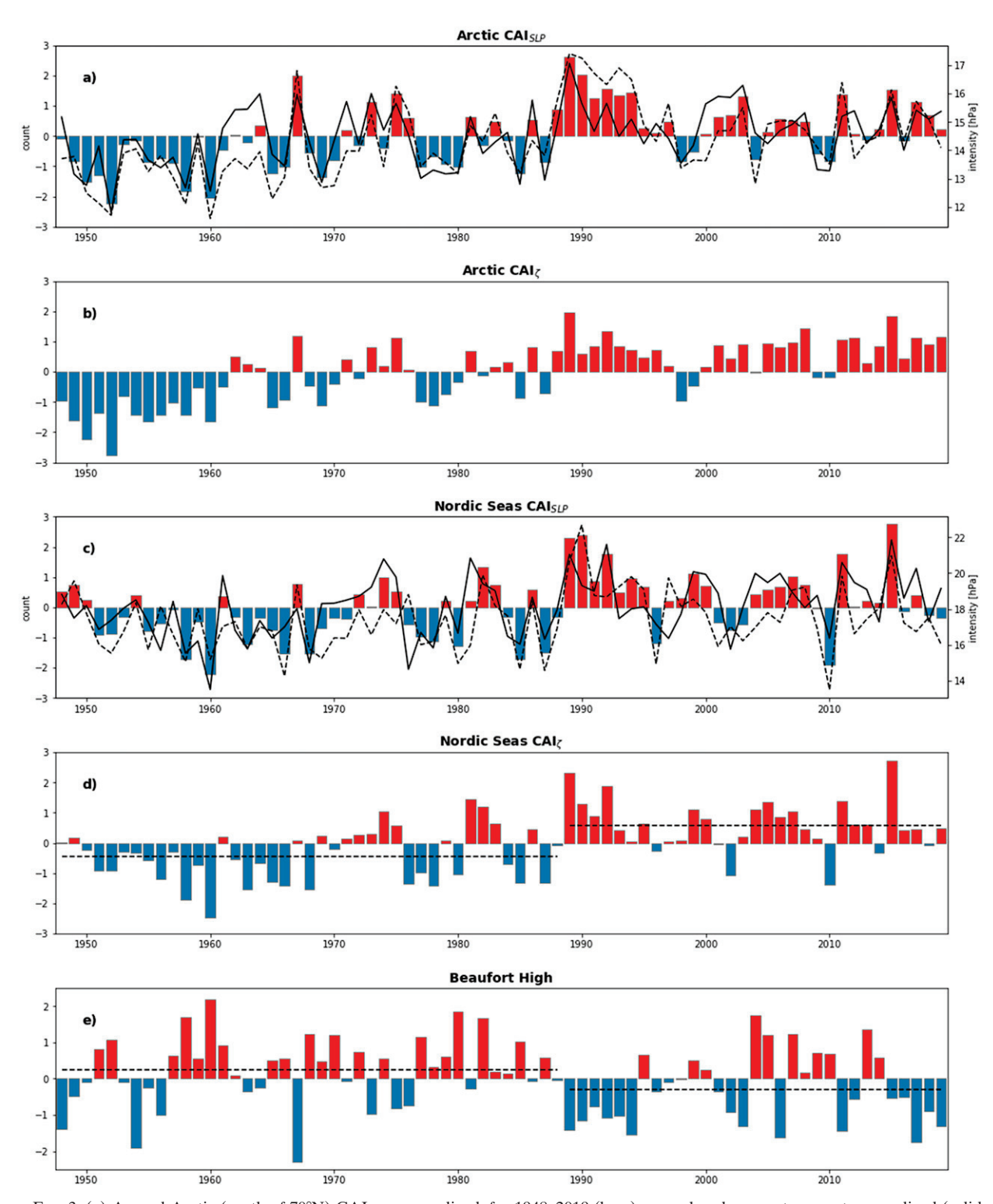


FIG. 3. (a) Annual Arctic (north of 70°N) CAI_{SLP}, normalized, for 1948–2019 (bars); annual cyclone center count, normalized (solid black line); and annual mean cyclone intensity (dashed black line). (b) Annual Arctic CAI $_{\xi}$, normalized. (c) As in (a), but for the Nordic seas (60°–77.5°N, 27.5°N–30°E). (d) As in (b), but for the Nordic seas. (e) Beaufort high (in normalized units). Horizontal black dashed lines in (d) and (e) show the mean over 1948–88 and 1989–2019.

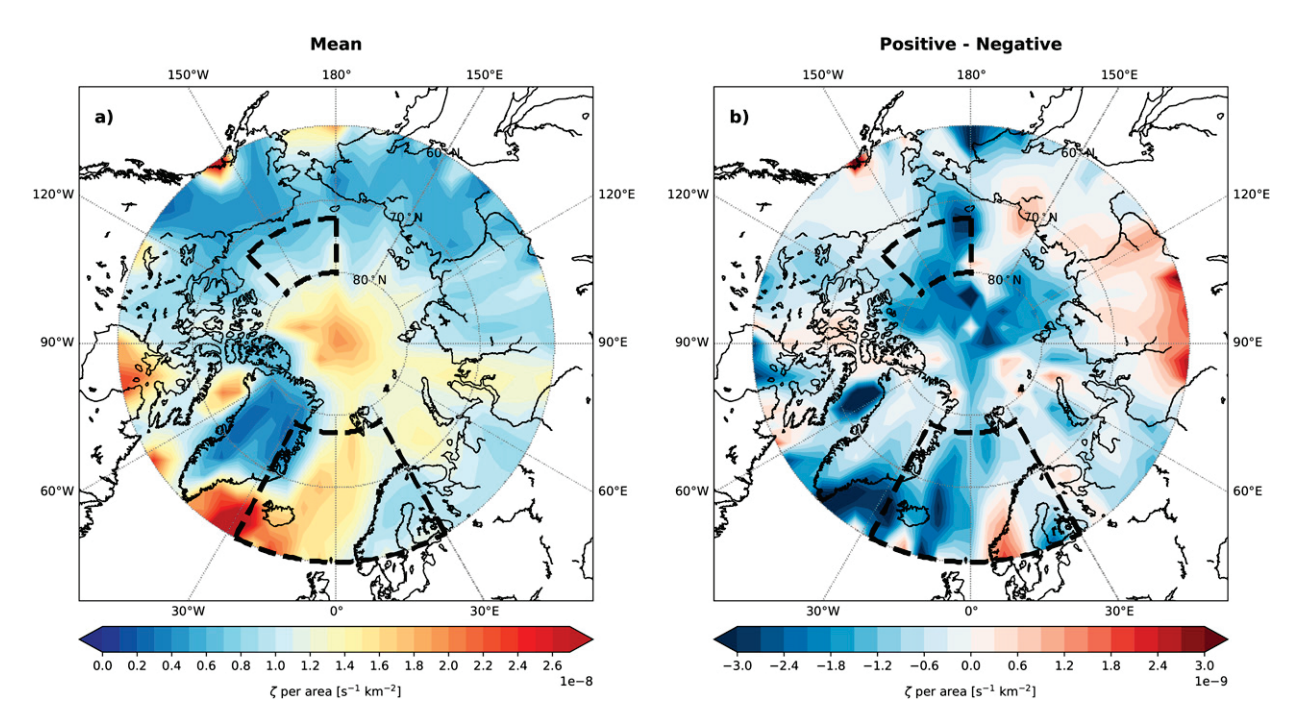


FIG. 4. (a) Relative vorticity ζ , summed over all cyclone centers occurring at each grid point during a given year and divided by the grid cell area, averaged over 1948–2019. (b) As in (a), but showing the difference between the means over positive and negative years of the BH (defined by exceedances of 0.5 standard deviations of the mean; colored bars in Fig. 1c). When the BH is relatively strong (i.e., positive), there is a reduction of cyclone activity (i.e., positive vorticity) over much of the Arctic, particularly the Nordic seas region. The Beaufort high and Nordic seas are defined by the black-outlined boxes.

the duration of each cyclone, remained nearly constant. However, the mean vorticity of Nordic seas cyclones when they cross into the Arctic increased by about $\sim\!10\%$. Furthermore, there was a relatively higher proportion of cyclones in the west cluster (compared to the east) in the 1989–2019 period, whereas cyclones in the east cluster dominated the 1948–88 period (Fig. 2c). In concert with this increase in cyclone activity, the BH decreased by about 0.5 standard deviations ($\sim\!1\,\mathrm{hPa}$) between these two periods (Fig. 3e).

5. Summary and discussion

Anticyclonic winds associated with the BH are a driver of the Beaufort Gyre circulation, which has considerable implications for the Arctic–subarctic freshwater budget. Extratropical cyclones play a role in the Arctic SLP field including the BH. Our identification and tracking of cyclones north of 60°N during 1948–2019 shows that the strength of the BH is associated with the intrusion into the Arctic interior of cyclones comprising the Icelandic low. This westward pathway is one of two principal pathways of Nordic seas cyclones; cyclones following an eastward trajectory remain confined to the Arctic periphery.

Using CAIs that reflect multiple properties of cyclone activity, we demonstrate a significant anticorrelation between Nordic seas cyclone activity and the BH during 1948–2019. In a sign of changing atmospheric forcing, Arctic and Nordic seas cyclone activity has exhibited a regime shift, from weaker activity during 1948–88 to stronger activity during 1989–2019;

there is also some suggestion, albeit not statistically robust, that the frequency of cyclones propagating along the westward pathway has increased between these two time periods. Also, between these two time periods and consistent with the relationships inferred here, the BH transitioned to a weaker state. Notably, the BH has been weaker than average during every year since 2015.

Understanding the fate of Beaufort Gyre freshwater under continued Arctic change is an essential element of viable climate projections. Ocean dynamics and change will depend on changes in the intensities and interactions of the main atmospheric centers of action, the BH and the Icelandic low. Sea ice has a role to play in these dynamics. For example, Moore et al. (2018) suggested that BH weakening in winter 2017 was related to anomalously low sea ice in the Barents Sea in fall and winter 2016. They argued that the reduced sea ice extent led to intensified air-sea heat fluxes that favored cyclone activity. A thermal low over the Barents Sea along with anomalous upperlevel circulation favored the penetration of North Atlantic cyclones into the Arctic interior. An additional complicated interrelationship that cannot be discounted is between changing sea ice in the Beaufort Gyre region and the changing strength of the BH. Coupled model results indicate that relatively low sea ice extents in fall may result in a relatively weaker BH, a consequence of unstable atmospheric boundary layers that form cyclonic circulations (Urrego-Blanco et al. 2019).

Under a scenario in which Arctic cyclone activity continues to increase in a warming climate, the BH would be expected to

experience less frequent positive anomalies, leading to a reduction of the anticyclonic upper-ocean circulation and of the Beaufort Gyre's freshwater reservoir. However, since 2015, the BH has been weak while the Beaufort Gyre has continued to accumulate freshwater (Proshutinsky et al. 2019). This suggests that other processes (e.g., the ongoing loss of sea ice and changes in freshwater availability) may be counteracting the reduction in anticyclonic atmospheric forcing, and these factors and their interactions need to be considered in assessing future Arctic Ocean dynamics and freshwater change.

Acknowledgments. Author J. S. Kenigson acknowledges the support of the Yale Institute for Biospheric Studies (YIBS) Donnelley Fellowship. Author M.-L. Timmermans acknowledges funding provided by the National Science Foundation Office of Polar Programs under award 1950077. We appreciate helpful exchanges with Gian A. Villamil-Otero in clarifying the cyclone identification algorithm.

Data availability statement. The NCEP-NCAR Reanalysis I SLP and wind fields are obtained from the NOAA Physical Sciences Laboratory (https://psl.noaa.gov/data/gridded/data.ncep. reanalysis.html). The AO index is obtained from NOAA (https://www.ncdc.noaa.gov/teleconnections/ao/).

REFERENCES

- Bell, G. D., and L. F. Bosart, 1989: A 15-year climatology of Northern Hemisphere 500 mb closed cyclone and anticyclone centers. *Mon. Wea. Rev.*, **117**, 2142–2164, https://doi.org/10.1175/1520-0493(1989)117<2142:AYCONH>2.0.CO;2.
- Chang, E. K., and A. M. Yau, 2016: Northern Hemisphere winter storm track trends since 1959 derived from multiple reanalysis datasets. *Climate Dyn.*, 47, 1435–1454, https://doi.org/10.1007/ s00382-015-2911-8.
- Garyfallidis, E., M. Brett, M. M. Correia, G. B. Williams, and I. Nimmo-Smith, 2012: Quickbundles, a method for tractography simplification. *Front. Neurosci.*, 6, 175, https://doi.org/ 10.3389/fnins.2012.00175.
- Gulev, S., O. Zolina, and S. Grigoriev, 2001: Extratropical cyclone variability in the Northern Hemisphere winter from the NCEP/NCAR reanalysis data. *Climate Dyn.*, 17, 795–809, https://doi.org/10.1007/s003820000145.
- Haine, T. W., and Coauthors, 2015: Arctic freshwater export: Status, mechanisms, and prospects. *Global Planet. Change*, **125**, 13–35, https://doi.org/10.1016/j.gloplacha.2014.11.013.
- Harvey, B., P. Cook, L. Shaffrey, and R. Schiemann, 2020: The response of the Northern Hemisphere storm tracks and jet streams to climate change in the CMIP3, CMIP5, and CMIP6 climate models. J. Geophys. Res. Atmos., 125, e2020JD032701, https://doi.org/10.1029/2020JD032701.
- Hori, M. E., J. Inoue, and T. Kikuchi, 2015: The role of cyclone activity in the interannual variability of the summertime Beaufort High. SOLA, 11, 104–107, https://doi.org/10.2151/ sola.2015-025.
- Kalnay, E., and Coauthors, 1996: The NCEP/NCAR 40-Year Reanalysis Project. *Bull. Amer. Meteor. Soc.*, **77**, 437–471, https://doi.org/10.1175/1520-0477(1996)077<0437:TNYRP>2. 0.CO;2.
- McCabe, G. J., M. P. Clark, and M. C. Serreze, 2001: Trends in Northern Hemisphere surface cyclone frequency and

- intensity. *J. Climate*, **14**, 2763–2768, https://doi.org/10.1175/1520-0442(2001)014<2763:TINHSC>2.0.CO;2.
- Moore, G., A. Schweiger, J. Zhang, and M. Steele, 2018: Collapse of the 2017 winter Beaufort High: A response to thinning sea ice? *Geophys. Res. Lett.*, 45, 2860–2869, https://doi.org/ 10.1002/2017GL076446.
- NCAR, 2019: The NCAR Command Language (version 6.6.2). UCAR/NCAR/CISL/TDD Doc., https://doi.org/10.5065/D6WD3XH5.
- NOAA, 2020: Monthly mean AO index. NOAA National Weather Service Climate Prediction Center, accessed 4 August 2020, http://www.cpc.ncep.noaa.gov.
- Proshutinsky, A., and Coauthors, 2009: Beaufort Gyre freshwater reservoir: State and variability from observations. *J. Geophys. Res.*, **114**, C00A10, https://doi.org/10.1029/2008JC005104.
- ——, D. Dukhovskoy, M.-L. Timmermans, R. Krishfield, and J. L. Bamber, 2015: Arctic circulation regimes. *Philos. Trans. Roy. Soc.*, A373, 20140160, https://doi.org/10.1098/RSTA. 2014.0160.
- —, and Coauthors, 2019: Analysis of the Beaufort Gyre freshwater content in 2003–2018. J. Geophys. Res. Oceans, 124, 9658–9689, https://doi.org/10.1029/2019JC015281.
- Rudeva, I., and S. K. Gulev, 2011: Composite analysis of North Atlantic extratropical cyclones in NCEP–NCAR reanalysis data. Mon. Wea. Rev., 139, 1419–1446, https://doi.org/10.1175/ 2010MWR3294.1.
- Sepp, M., and J. Jaagus, 2011: Changes in the activity and tracks of Arctic cyclones. *Climatic Change*, **105**, 577–595, https://doi.org/10.1007/s10584-010-9893-7.
- Serreze, M. C., 1995: Climatological aspects of cyclone development and decay in the Arctic. *Atmos.—Ocean*, 33, 1–23, https://doi.org/10.1080/07055900.1995.9649522.
- —, and R. G. Barry, 1988: Synoptic activity in the Arctic Basin, 1979–85. J. Climate, 1, 1276–1295, https://doi.org/10.1175/ 1520-0442(1988)001<1276:SAITAB>2.0.CO;2.
- —, and A. P. Barrett, 2008: The summer cyclone maximum over the central Arctic Ocean. J. Climate, 21, 1048–1065, https:// doi.org/10.1175/2007JCLI1810.1.
- —, and —, 2011: Characteristics of the Beaufort Sea high.
 J. Climate, 24, 159–182, https://doi.org/10.1175/2010JCLI3636.1.
- —, J. Box, R. Barry, and J. Walsh, 1993: Characteristics of Arctic synoptic activity, 1952–1989. *Meteor. Atmos. Phys.*, **51**, 147– 164, https://doi.org/10.1007/BF01030491.
- —, F. Carse, R. G. Barry, and J. C. Rogers, 1997: Icelandic low cyclone activity: Climatological features, linkages with the NAO, and relationships with recent changes in the Northern Hemisphere circulation. *J. Climate*, 10, 453–464, https://doi.org/10.1175/1520-0442(1997)010<0453:ILCACF>2.0.CO;2.
- Simmonds, I., C. Burke, and K. Keay, 2008: Arctic climate change as manifest in cyclone behavior. J. Climate, 21, 5777–5796, https://doi.org/10.1175/2008JCLI2366.1.
- Sorteberg, A., and J. E. Walsh, 2008: Seasonal cyclone variability at 70°N and its impact on moisture transport into the Arctic. *Tellus*, **60A**, 570–586, https://doi.org/10.1111/j.1600-0870.2008.00314.x.
- —, N. G. Kvamsto, and O. Byrkjedal, 2005: Wintertime Nordic Seas cyclone variability and its impact on oceanic volume transports into the Nordic Seas. *The Nordic Seas: An Integrated Perspective, Geophys. Monogr.*, Vol. 158, Amer. Geophys. Union, 137–156, https://doi.org/10.1029/158GM10.
- Thompson, D. W., and J. M. Wallace, 1998: The Arctic Oscillation signature in the wintertime geopotential height and temperature fields. *Geophys. Res. Lett.*, 25, 1297–1300, https://doi.org/ 10.1029/98GL00950.

- Urrego-Blanco, J. R., E. C. Hunke, and N. Urban, 2019: Emergent relationships among sea ice, longwave radiation, and the Beaufort high circulation exposed through parameter uncertainty analysis. *J. Geophys. Res. Oceans*, **124**, 9572–9589, https://doi.org/10.1029/2019JC014979.
- Villamil-Otero, G. A., J. Zhang, J. He, and X. Zhang, 2018: Role of extratropical cyclones in the recently observed increase in poleward moisture transport into the Arctic Ocean. Adv. Atmos. Sci., 35, 85–94, https://doi.org/10.1007/s00376-017-7116-0.
- Yin, J. H., 2005: A consistent poleward shift of the storm tracks in simulations of 21st century climate. *Geophys. Res. Lett.*, **32**, L18701, https://doi.org/10.1029/2005GL023684.
- Zhang, X., M. Ikeda, and J. E. Walsh, 2003: Arctic sea ice and freshwater changes driven by the atmospheric leading mode in a coupled sea iceocean model. J. Climate, 16, 2159–2177, https://doi.org/10.1175/2758.1.
- —, J. E. Walsh, J. Zhang, U. S. Bhatt, and M. Ikeda, 2004: Climatology and interannual variability of Arctic cyclone activity: 1948–2002. *J. Climate*, 17, 2300–2317, https://doi.org/10.1175/1520-0442(2004)017<2300:CAIVOA>2.0.CO;2.